International Journal of Pharmaceutics 419 (2011) 296–307

Contents lists available at ScienceDirect

International Journal of Pharmaceutics

journal homepage: www.elsevier.com/locate/ijpharm

Pharmaceutical Nanotechnology

Characterization and evaluation of chitosan nanoparticles for dopamine brain delivery

Adriana Trapani[a], Elvira De Giglio[b], Damiana Cafagna[b], Nunzio Denora[a], Gennaro Agrimi[c], Tommaso Cassano[d], Silvana Gaetani[e], Vincenzo Cuomo[e], Giuseppe Trapani[a,*]

[a] Pharmaco-Chemistry Department, University of Bari, Via Orabona 4, 70125 Bari, Italy
[b] Department of Chemistry, University of Bari, Via Orabona 4, 70125 Bari, Italy
[c] Pharmaco-Biology Department, University of Bari, Via Orabona 4, 70125 Bari, Italy
[d] Department of Biomedical Sciences, University of Foggia, V.le L. Pinto 1, 71100 Foggia, Italy
[e] Department of Physiology and Pharmacology "V. Erspamer", Sapienza University of Rome, P.le A. Moro 5, 00185 Rome, Italy

ARTICLE INFO

Article history:
Received 22 April 2011
Received in revised form 21 July 2011
Accepted 22 July 2011
Available online 28 July 2011

Keywords:
Dopamine
Chitosan nanoparticles
XPS
Transport studies
Brain microdialysis

ABSTRACT

The aim of this study was to characterize nanoparticles (NPs) composed of chitosan (CS) and evaluate their potential for brain delivery of the neurotransmitter Dopamine (DA). For this purpose, CS based NPs were incubated with DA at two different concentrations giving rise to nanocarriers denoted as DA/CSNPs (1) and DA/CSNPs (5), respectively. X-ray Photoelectron Spectroscopy (XPS) analysis confirmed that DA was adsorbed onto the external surface of such NPs. The cytotoxic effect of the CSNPs and DA/CSNPs was assessed using the MTT test and it was found that the nanovectors are less cytotoxic than the neurotransmitter DA after 3 h of incubation time. Transport studies across MDCKII-MDR1 cell line showed that DA/CSNPs (5) give rise to a significant transport enhancing effect compared with the control and greater than the corresponding DA/CSNPs (1). Measurement of reactive oxygen species (ROS) suggested a low DA/CSNPs neurotoxicity after 3 h. *In vivo* brain microdialysis experiments in rat showed that intraperitoneal acute administration of DA/CSNPs (5) (6–12 mg/kg) induced a dose-dependent increase in striatal DA output. Thus, these CS nanoparticles represent an interesting technological platform for DA brain delivery and, hence, may be useful for Parkinson's disease treatment.

1. Introduction

Parkinson's disease (PD) is the most common neurodegenerative movement disorder, primarily associated with degeneration of the pigmented neurons in the *substantia nigra*, resulting in decreased nigrostriatal availability of the neurotransmitter dopamine (DA) (Pahwa and Koller, 1998). For the treatment of PD, the clinical efficacy of L-Dopa is well established because it is carrier-mediated transported across blood–brain barrier (BBB) and converted in the brain to DA which, in turn, is not able itself to overcome the barrier. The BBB represents an effective obstacle for the delivery of neuroactive agents to the central nervous system (CNS) and it makes the treatment of many CNS diseases difficult to achieve. The hydrophilic feature of DA as well as its high hydrogen bonding potential still constitutes a challenge for supplying the neurotransmitter to the CNS. Moreover, it should be also considered that (i) DA may be a source of a dopaminergic neurotoxin such as 6-hydroxydopamine (6-OHDA) which is involved in the progression of the disease. In fact, it has been suggested that DA can induce the degeneration of cultured dopaminergic neurons, enhancing oxidative stress with increased reactive oxygen species (ROS) formation (Jellinger et al., 1995); (ii) DA is a sensitive molecule since it can be oxidized to give polymerized compounds (such as melanine compounds) through the formation of quinone intermediates (Enoch et al., 1994). For these reasons, the search for novel therapeutic strategies based on DA replacement therapy is still ongoing. For instance, recently, the so called "chemical approach" of prodrugs and/or codrugs led to the combination of L-Dopa with the antioxidant agent Glutathione in an attempt to limit the oxidative damage to the *substantia nigra* region of Parkinson's patients (Pinnen et al., 2007). On the other hand, even though the prodrug approach work quite well to deliver DA, also the so called "particulate based approach", consisting of micro and nanoparticles (NPs) as drug delivery systems, has been exploited for anti-Parkinson agents (Demirel et al., 2001). More recently, DA-loaded cellulose acetate phthalate NPs have been investigated by Pillay et al. (2009) and these particulate systems were used for an invasive administration route (i.e., the intratecal

* Corresponding author at: Dipartimento Farmaco-Chimico, Facoltà di Farmacia, Università degli Studi di Bari, Via Orabona 4, 70125 Bari, Italy. Tel.: +39 080 5442764; fax: +39 080 5442754.
E-mail address: trapani@farmchim.uniba.it (G. Trapani).

0378-5173/$ – see front matter © 2011 Elsevier B.V. All rights reserved.
doi:10.1016/j.ijpharm.2011.07.036

implantation). To the best of our knowledge, the paper by Pillay et al. (2009) is the first report describing DA loading in polymeric NPs. The approach to overcome the obstacle of BBB through the use of nanodevices represents one the fields of great interest in modern pharmaceutical research devoted to improve the treatment of brain diseases (Paolino et al., 2011). These systems may have some advantages over the conventional formulations (e.g., prodrugs and/or codrugs based formulations) such as the ability to circumvent P-glycoprotein (P-gp)-mediated resistance (Cho et al., 2008), the possibility of bypassing the BBB without structural modifications and the possibility of employing biocompatible and biodegradable materials. It motivated our interest to further explore the potential of nanoparticulate system approach in delivering DA.

Currently, among several NP prototypes prepared from biodegradable polymers, NPs based on the cationic polysaccharide chitosan (CS) have shown particularly promising results due to the polycation intrinsic properties including low toxicity, excellent biocompatibility, high loading and good delivery ability for hydrophilic molecules (Csaba et al., 2006; Ieva et al., 2009). In the literature, brain delivery applications of CS NPs include CS based nanospheres enabling to deliver hydrophilic anticancer drug such as doxorubicin into the mice brain (Du et al., 2007) and, moreover, the Tween 80 coating of CS NPs was demonstrated to maximize the translocation of these nanosystems from blood to brain (Sheetal et al., 2005). Furthermore, it has been well established that CS is capable of opening the tight junctions of epithelial cells and it can improve the uptake of hydrophilic drugs including peptides (Mao et al., 2010). Moving from this background, in the present work we aimed to investigate the potential of DA loaded CS NPs to be administered by parenteral route and able to overcome the BBB and deliver DA to the brain. We hypothesized, indeed, that the positive surface charge of these CS NPs would be favourable for their transport across the BBB by adsorptive-mediated transcytosis (AMT). AMT is a vesicular transport route of cationic substances through the BBB and, unlike receptor-mediated transcytosis (RMT), it does not require specific binding sites on cell surfaces but involves electrostatic interactions between polycationic substances and negative charges on the endothelial surface (Hervé et al., 2008). For the above mentioned purpose, DA loaded CS based NPs were prepared and extensively characterized *in vitro* with regard to their physicochemical properties, their capacity to load and release DA, interaction with and transport across MDCKII-MDR1 cell line, taken as an *in vitro* model of BBB. In addition, an *in vivo* biodistribution study using microdialysis, a well-established sampling method for determining neurotransmitter concentrations in the brain of freely-moving animals, was performed. The results obtained are herein reported and discussed.

2. Materials and methods

2.1. Materials and animals

The following chemicals were obtained from commercial sources and used as received. Chitosan hydrochloride (UP CL 113, M_w 110 kDa, deacetylation degree 86% according to manufacturer instructions) was purchased from Pronova Biopolymer (Norway). Dopamine hydrochloride, glycerol (over 99.5% purity), 2′,7′-dichlorodihydrofluorescein diacetate, 6-hydroxydopamine (6-OHDA), fluorescein-dextran 4000 (FD4), fluorescein isothiocyanate (FITC) and pentasodium tripolyphospate (TPP) were purchased from Sigma–Aldrich, Italy. Ultrapure water (Carlo Erba, Italy) was used throughout the study. All other chemicals were reagent grade. Madin–Darby canine kidney (MDCKII-MDR1) cells (passages 6–18) were kindly donated by the Netherlands Cancer Institute and grown in Dulbecco's modified Eagle's medium (DMEM) containing glucose (4.5 g/L) (Euroclone, Italy) supplemented with 10% fetal bovine serum (Euroclone, Italy) penicillin (100 U/mL), streptomycin (100 μg/mL) and 2 mM L-glutamine. The cells were kept at 37 °C in an atmosphere of 95% air and 5% CO_2.

Animal care and all experiments were conducted in accordance with the guidelines of the European Communities Council Directive of 24 November 1986 (86/609/EEC) and the Italian Department of Health (D.L. 116/92), and approved by the Institutional Animal Care and Use Committees of the University of Foggia, Italy. All efforts were made to minimize animal suffering and to reduce the number of animals used in the study. Male Wistar rats (225–250 g; Harlan, San Pietro al Natisone, Udine, Italy) were housed on 12-h dark-light cycle, at 22 ± 1° C with food and water available *ad libitum* and habituated to housing conditions for 1 week before the experiments.

2.2. Nanoparticle preparation

Chitosan NPs in the presence and in the absence of DA were prepared according to a modified ionic gelation method (Trapani et al., 2008). (a) *Unloaded CS Nanoparticles*: 1.5 mL of a CS solution (0.20%, w/v, in acetic acid 0.1%, v/v) was maintained under magnetic stirring prior to the addition of 1.6 mL of TPP aqueous solution (0.07%, w/v) leading to NPs formation. The final CS/TPP mass ratio was equal to 2.7:1 (w/w). Herein, unloaded chitosan NPs were denoted as "CSNPs". (b) *DA adsorbing CSNPs* were prepared as follows. To 1 mL of an aqueous solution of DA at the concentration of 1 mg/mL or 5 mg/mL, 0.5 mL of the previously described CSNPs were added and maintained to incubate at 25 °C in a water bath for 3 h under mild stirring (50 oscillations/min). This process was conceived to lead to adsorption of DA onto the external surface of CSNPs. Herein, DA-adsorbing chitosan NPs were labelled as "DA/CSNPs (1)" and "DA/CSNPs (5)" when the concentration of DA feeding solution was set equal to 1 and 5 mg/mL, respectively. Finally, for all formulations, the resulting NPs were isolated by centrifugation (16,000 × *g*, 45 min, Eppendorf 5415D, Eppendorf, Germany) and resuspended in ultrapure water by manual shaking.

2.3. Physicochemical characterization of nanoparticles

Particle size and polydispersity index (PI) of all tested NPs were determined in double distilled water by photon correlation spectroscopy (PCS) using a Zetasizer NanoZS (ZEN 3600, Malvern, UK). The determination of the ζ-potential was performed using laser Doppler anemometry (Zetasizer NanoZS, ZEN 3600, Malvern, UK) after dilution with 1 mM KCl and following a previously reported procedure (Lopedota et al., 2009).

2.4. HPLC analysis

High-performance liquid chromatography (HPLC) analyses of DA were performed with a Waters (Waters Corp., Milford, MA) Model 600 pump equipped with a Waters 2996 photodiode array detector, a 20 μL loop injection autosampler (Waters 717 plus), and processed by Empower™ Software Build. For analysis, a reversed phase Synergy Hydro-RP (25 cm × 4.6 mm, 4 μm particles; Phenomenex, Torrance, CA) column in conjunction with a precolumn C18 insert was eluted with 0.020 M potassium phosphate buffer (pH 2.8) in isocratic mode. The flow rate was maintained at 0.9 mL/min. Standard calibration curves for DA determination were prepared at 280 nm wavelength in double distilled water and calibration curve linearity ($r^2 > 0.999$) was maintained over the range of concentrations tested (4.75×10^{-4} to 1.5×10^{-5} M). The retention time of DA was 8 min.

For cell experiments, the HPLC analysis of diazepam (DZ) was carried out by a reversed phase Varian column (15 cm × 4.6 mm,

5 μm particles) in conjunction with a precolumn C18 insert was eluted with 80:20 (v:v) methanol:water in isocratic mode. The flow rate of 1.0 mL/min was maintained and the column effluent was monitored continuously at 242 nm. The retention time of DZ was 4 min.

For microdialysis studies, the extracellular level of DA was determined by HPLC using a ODS Hypersil (Thermo Fisher Scientific, Milan, Italy) 150-mm × 3-mm column (5-μm particle size) with a Unijet cell (BAS, Bioanalytical Systems, Kenilworth Warwickshire, United Kingdom) equipped with a 6-mm diameter glassy carbon electrode (set at +650 mV) and connected to an electrochemical amperometric detector (INTRO, Antec Leyden, The Netherlands), as previously described (Cassano et al., 2009). The flow rate of the mobile phase [85 mM sodium acetate, 0.34 mM EDTA, 15 mM sodium chloride, 0.81 mM octanesulfonic acid sodium salt, 5% methanol (v/v), pH 4.85] was 700 μL/min and the total runtime was 15 min.

2.5. Determination of DA association efficiency

The association efficiency (AE) of DA to the particles was calculated by an indirect method. DA/CSNPs (1) and DA/CSNPs (5) were isolated from unbound DA by centrifugation (16,000 × *g*, 45 min, Eppendorf 5415D, Eppendorf, Germany), and free DA in the supernatant was quantified by HPLC as described above. Experiments were performed in triplicate and the association efficiency was calculated as follows (Eq. (1)):

$$\%\,\mathrm{AE} = 100 \times \frac{\text{Total DA} - \text{Free DA}}{\text{Total DA}} \quad (1)$$

To determine NPs process yield, batches of NPs were centrifuged (16,000 × *g*, 45 min) and the pellet was then lyophilized for 48 h and weighed. The process yield was calculated as follows (Eq. (2)):

$$\text{Process yield}\ (\%) = \frac{\text{particles weight}}{\text{weight of total components}} \times 100 \quad (2)$$

2.6. Atomic force microscopy (AFM) observations

AFM was carried out to characterize the morphology of CSNPs. The AFM images were obtained using a XE-100 (Park Systems, Suwon, Korea) instrument in non-contact mode and using a PPP-NCHR cantilever with 330 kHz resonant frequency. Scan speed was between 0.5 and 1.5 Hz using the adaptive scan mode function set in the software. All the images are 256 × 256 data points. For AFM visualization, a drop of diluted nanoparticle suspension (0.1 mg/mL) was drop casted onto a flat microscopy glass; then, after overnight evaporation, the sample was processed directly on the AFM scanner. To get high resolution images of nanoparticles deposited on the substrate, typically PPP-NCHR silicon cantilevers with a length of 125 μm were used with resonance frequency of about 270 kHz and a nominal force constant around 42 N/m. The tip to sample distance was kept constant using the amplitude feedback function in attractive forces regimen to prevent the damage of the NPs.

2.7. XPS analysis

X-ray photoelectron spectroscopy (XPS) analysis was performed with a ThermoVG Thetaprobe spectrometer (Thermo Fisher Scientific, Inc., Waltham, MA, USA) equipped with a microspot monochromatized Al Kα source. The Al Kα line (1486.6 eV) was used throughout. Survey scans (binding energy range 0–1200 eV, FAT mode, pass energy = 150 eV) and detailed spectra (FAT mode, pass energy = 50 eV) were recorded. Data were analyzed using the Advantage software package Version 3.99. The sample charging effects were minimized with a low-energy flood gun. Charge referencing was done by setting the lower binding energy C1s photopeak at 285.0 eV, C1s hydrocarbon peak. Quantification was done by peak area comparison of data from different elements and was enabled by correction with empirically derived atomic sensitivity factors. Data were averaged over at least three samples analyzed.

2.8. DA/CSNP (5) formulation stability

The size stability of DA/CSNPs (5) was tested by incubation in MDCKII-MDR1 cell culture medium, in that used for microdialysis studies and in pure water. The compositions of these media are reported below. In these studies, nanoparticle suspensions were diluted in the media in a concentration range detectable by PCS and maintained at 37 °C under agitation (100 rpm). At different time points NP size was measured by PCS up to 24 h. Each experiment was performed in triplicate.

2.9. In vitro release study

In vitro release studies of DA/CSNPs (1) and DA/CSNPs (5) were carried out in phosphate buffer saline (PBS, pH 7.4) medium without enzymes for 48 h, and performed according to USP XXVI recommendations. Freshly prepared CSNPs were isolated in Eppendorf tubes with a 10 μL-glycerol bed in the bottom of the tube, set to help the resuspension of the formulation. The amount of particles was adjusted to obtain a maximum DA concentration in the range 0.1–2.0 mg/mL. In screw-capped test tubes, each formulation was resuspended in 0.4 mL of distilled water and the resulting resuspended formulation was mixed with 3 mL of release medium (PBS, pH 7.4) and incubated at 37 °C under mechanical agitation (100 oscillations/min). At appropriate time intervals, an aliquot (0.3 mL) was withdrawn and centrifuged (16,000 × *g*, 40 min, Eppendorf 5415D, Eppendorf, Germany). The initial volume of release medium was maintained by refilling 0.3 mL of the same medium after each withdrawal. The supernatant was analyzed for DA content by HPLC as described above. Each experiment was performed in triplicate.

2.10. MTT test on MDCKII-MDR1 cell line

In vitro cytotoxicity of free DA, unloaded NPs and DA adsorbing NPs was evaluated using the MTT assay. MDCKII-MDR1 cells were seeded into 96-well microtiter plates (3596 Cell Colture Microplate Corning Costar Corp., Germany) at a density of 3×10^4 cells/cm^2. After 24 h, the culture medium was replaced with 100 μL/well of serial dilutions of the samples in complete medium (*n* of wells per NP concentration = 8). The cells were exposed to free DA (1000–0.2 μg/mL), unloaded CSNPs (particle range concentration 20–0.02 μg/mL) and DA/CSNPs (1)/DA/CSNPs (5) (particle range concentration 10–0.2 μg/mL corresponding to a DA concentration in the range 2–0.2 μg/mL) for 3 and 24 h. Sodium dodecyl sulfate (SDS) was used as positive control at the concentration of 2% (w/v) in complete cell medium. After an incubation period of 3 h (or 24 h), the samples were aspirated. Separately, 3-(4,5-dimethyl-thiazol-2-yl)-2,5-diphenyl tetrazolium bromide (MTT; Sigma–Aldrich, Italy) was dissolved in phosphate buffered saline at 5 mg/mL and 100 μL of the final concentration of 0.5 mg of MTT/mL in FBS-free DMEM were added to each well. After an incubation time of 4 h, the unreacted dye was removed by aspiration and the purple formazan product was dissolved in 100 μL/well dimethyl sulfoxide and quantitated by a plate reader (Victor^{TM} X3, 2030 Multilabel Reader, Perkin Elmer, Italy) at wavelength of 570 nm. The relative cell viability (%) related to control wells containing cell culture medium without sample was calculated by (A test/A control) × 100. The IC_{50} was defined as the sample concentration inhibiting 50% cell

viability. The percentages of cell viability were corrected for the intrinsic fluorescence due to DA in cell medium in the absence of MDCKII-MDR1 cells. For quantification of the intrinsic fluorescence, the DA content was calculated by comparing the results to that of a standard curve obtained using standard DA solutions. Linearity was checked in the range from 0.2 μg/mL to 3000 μg/mL.

2.11. Association of FITC-DA/CSNPs (5) by MDCKII-MDR1 cell line (flow cytometry analysis)

To demonstrate the interaction of DA/CNSPs with MDCKII-MDR1 cell line, CS was labelled with fluorescein isothiocyanate (FITC) following reported procedures with slight modifications (Park et al., 2006). Briefly, 80 mg of the polymer was dissolved in water under acidic conditions due to the addition of 4 mL of 1 N HCl, and, thereafter, the pH was adjusted to 6.5 with 3 mL of 1 N NaOH. 0.4 mL of FITC solution (20 mg/mL in ethanol) were added to above prepared CS solution, the resulting mixture was stirred at room temperature for 24 h. Then, the mixture was dialyzed in water using dialysis tubing (SpectraPore® Dialysis MWCO 10,000) for 3 days and freeze dried for at least 48 h. All the preparative steps were carried out under light protection. The FITC DA/CSNPs (5) were formed by the same procedure of unlabelled DA/CSNPs (5).

The association of FITC-DA/CSNPs (5) with MDCKII-MDR1 cells was studied by flow cytometry measuring the green fluorescence of the cells after incubation with the labelled particles. MDCKII-MDR1 cells were plated at a density of 2.5×10^4 cells/cm^2. When the cells reached about 80% confluence, they were treated with 4 μg/mL of FITC-DA/CSNPs (5) for 15 min, 60 min and 180 min. The cells were washed with Dulbecco's modified phosphate buffer saline (D-PBS, pH 7.4), trypsinized and centrifuged at 1000 rpm for 5 min to obtain a cell pellet. The cells were washed twice with ice cold D-PBS and analyzed using a flow cytometer (Coulter EPICS Elite ESP) equipped with a 488 nm 15-mW argon-ion laser, dichroic mirror (502 Cp), and band-pass filter (530/30) by counting 10,000 events. The instrument was adjusted with non-treated cells. The mean fluorescence intensity of the cells was calculated using histogram plot.

2.11.1. Transport of DA and DA/CSNPs across MDCKII-MDR1 cell line

MDCKII-MDR1 cells were grown to confluence for 8 days. Cells were seeded at a density of 5×10^4 cells/cm^2 on uncoated polycarbonate Transwell™ filter inserts (3402 Corning Costar Corp., Germany, 3 μm pore size, area: 1.12 cm^2) and the medium was changed every other day. On the day of the experiment, cells were rinsed twice and equilibrated at 37 °C for 30 min with the assay medium. The assay medium had the following composition: K_2HPO_4 0.4 mM, $NaHCO_3$ 25.0 mM, KCl 3.0 mM, $MgSO_4$ 1.2 mM, $CaCl_2$ 1.4 mM, NaCl 122.0 mM and glucose 10.0 mM. The pH was adjusted to be 7.4 and the osmolarity was 300 mOsm/kg (Micro-Osmometer Automatic Type 13 RS, Hermann Roebling Messtechnik, Berlin, Germany). DA/CSNPs (1) and DA/CSNPs (5) were freshly prepared and resuspended in 1.8 mL of assay medium containing the paracellular marker FITC-dextran 4000 (FD4, 25 μM) and the transcellular marker diazepam (DZ, 75 μM) (Gaillard and de Boer, 2000). After the assay medium was aspirated, the cells were apically incubated with free DA (3 mg/mL) and NP suspensions loading 0.2 mg/mL of DA for 3 h at 37 °C. In the control wells, the same media without NPs and free DA were used. At $t = 0$, samples from the apical media were collected to precisely calculate the total amounts of DA, DZ and FD4 present in the apical chamber. At fixed times, withdrawals of 0.3 mL from the basolateral compartment were analyzed for DA, DZ and FD4 permeated. The permeated FD4 was assayed by fluorimetric assay (Victor™ X3, 2030 Multilabel Reader, Perkin Elmer, Italy, Excitation: 485 nm; Emission 535 nm).

The apparent permeability coefficient P_{app} was calculated using the following equation (Eq. (3)):

$$P_{app} = \frac{dQ}{dt}\left(\frac{1}{A} \times 60 \times c_0\right) \quad (3)$$

where dQ/dt is the permeability rate (mg/min), namely the amount of the analyte permeating the monolayer in time t (min) obtained from the permeation profiles; A is the diffusion area of the monolayer; c_0 is the initial analyte concentration (mg/mL). During the experiments, the integrity of the monolayers was checked by means of transepithelial electric resistance (TEER) measurements at prefixed times before and after the experiment using a volt ohmmeter (EVOM, World Precision Instruments, Germany) equipped with Endohm electrodes. The monolayers exhibiting 140–440 Ω cm^2 TEER were used for the experiments.

2.11.2. Transport FITC labelled unloaded CSNPs across MDCKII-MDR1 cell line

MDCKII-MDR1 cells were grown to confluence for 14 days. Cells were seeded at a density of 5×10^4 cells/cm^2 on uncoated polycarbonate Transwell™ filter inserts (3412 Corning Costar Corp., Germany, 0.4 μm pore size, area: 4.71 cm^2) and the medium was changed every other day. On the day of the experiment, cells were rinsed twice and equilibrated at 37 °C for 30 min with D-PBS. FITC labelled CSNPs were freshly prepared and centrifuged in order to remove free FITC. After the D-PBS was aspirated from the cells, FITC-CSNPs corresponding to 18 μM of FITC were apically incubated for 3 h at 37 °C. In the control wells, the same medium without NPs was used. At $t = 0$, samples from the apical media were collected to precisely calculate the total amounts of FITC present in the apical chamber. At fixed times, withdrawals of 0.5 mL from the basolateral compartment were analyzed by fluorimetric assay (Victor™ X3, 2030 Multilabel Reader, Perkin Elmer, Italy; Excitation: 485 nm and Emission 535 nm). The observed fluorescence intensities were corrected for cell medium background.

2.12. Fluorescence microscopy

Wide field fluorescence of cells was analyzed through an inverted Zeiss Axiovert 200 microscope (Zeiss, Milan, Italy) equipped with a 63×/1.4 oil objective. In particular, uptake of FITC-CSNPs into MDCKII-MDR1 cells was imaged 4 h after the treatment, whereas nuclei were labelled with 1 μg/mL DAPI both in control and in treated cells at the designated time after an incubation time of 30 min. Excitation of FITC-CSNPs and DAPI as well as the selection of their emission fluorescences was accomplished with appropriate filters mounted in Lambda 10-2 filter wheel controllers (Sutter Instruments, Novato, CA, USA). Fluorescence images were captured by a CoolSNAP HQ CCD camera (Roper Scientific, Trenton NJ) using the Metamorph 6.1 Software (Universal Imaging Corporation).

2.13. Determination of intracellular reactive oxygen species (ROS)

For measurement of intracellular ROS, MDCKII-MDR1 cells were seeded into 96-well microtiter plates (3596 Cell Colture Microplate Corning Costar Corp., Germany) at a density of 10^5 cells/cm^2. Just prior to the assay, the nutrient medium was removed and the cells were washed twice with D-PBS. To study whether CS NPs could prevent 6-hydroxydopamine (6-OHDA)-induced intracellular ROS production, the cells were preincubated with CSNPs, DA/CSNPs (1) and DA/CSNPs (5) for 3 and 24 h. Then, the cells were loaded with 5 μM of the oxidation-sensitive fluorescent probe, 2′,7′-dichlorodihydrofluorescein diacetate (DCFH-DAc), in DMSO solution at 37 °C in the dark (Puttonen et al., 2006). DCFH-DAc diffuses into the cell through the plasma membrane and is hydrolyzed by intracellular esterases to nonfluorescent DCFH.

Intracellular oxidation converts DCFH into the highly fluorescent 2′,7′-dichlorofluorescein (DCF). The fluorescence was measured by microplate reader (ex. 485 nm, em. 535 nm) after 15 min to ensure the uptake of the probe. The stock solution of 6-OHDA was made in ultrapure water and further diluted in PBS (pH 7.4). The loaded cells were treated with 6-OHDA (100 μM) and incubated at 37 °C in the dark for 10 min after which the fluorescence was measured as above. Fluorescent intensity was calculated as percent increase of fluorescent intensity when compared with 6-OHDA-treated cells [(fluorescent intensity of cells in the treated sample/fluorescent intensity of cells in the control sample) × 100].

2.14. Microdialysis and treatment schedule

DA/CSNPs freshly prepared were administered i.p. in a volume of 3 mL/kg of body mass. Animals were anesthetized with equithesin (3 mL/kg, i.p.) [Na-pentobarbital (0.972 g), chloral hydrate (4.251 g), magnesium sulfate (2.125 g), ethanol (12.5 mL), and propylene glycol (42.6 mL) in distilled water (total volume, 100 mL)] and positioned on a stereotaxic frame (Kopf Instruments, Tujunga, CA). A custom-made microdialysis probe of concentric design (AN69 Hospal S.p.A; 20 kDa cut-off; membrane length, 3-mm) was implanted into the striatum according to the following stereotaxic coordinates: AP +1.0, ML ±2.8 from bregma and DV −6.8 from dura (Paxinos and Watson, 1998). The microdialysis probe was fixed to the skull with stainless steel screws and methylacrylic cement. Twenty-four hours after surgery, the microdialysis probe was perfused with Krebs Ringer solution (NaCl 145 mmol/L, KCl 2.7 mmol/L, $CaCl_2 \cdot 2H_2O$ 1.2 mmol/L, $MgCl_2 \cdot 6H_2O$ 1 mmol/L, Na_2HPO_4 2 mmol/L, pH 7.4) at a constant flow rate of 2 μL/min. Perfusates were collected every 20 min into mini-vials containing 3 μL of 10% acetic acid. After a wash-out period of 2 h, 4 samples were collected to determine the baseline levels of the DA (no more than 10% difference among 4 consecutive samples). Rats were acutely treated with DA/CSNPs (5) (6–12 mg/kg, i.p.), or vehicle (CSNPs, i.p.) and consecutive microdialysate samples were collected every 20 min over a 4 h period. DA concentration, obtained from the same samples, were detected and quantified by HPLC. At the end of each experiment, the correct placement of dialysis probes was verified histologically.

2.15. Statistics

Data from different experimental groups were compared by a one-way analysis of variance (ANOVA) with $p < 0.05$ at 99% level of confidence (GraphPad Prism v. 4.00 GraphPad Software, Inc., San Diego, CA). Bonferroni post tests were used for post-hoc contrast.

Neurochemical data were expressed as percentages of baseline (±SEM), which was defined as the average of four consecutive samples with stable level of neurotransmitters before drug administration. Data were analyzed by two-way ANOVA for repeated measures with treatment (*tr*) as the between variable and time (*t*) as the within variable. Violations of the sphericity assumption were corrected using the Greenhouse–Geisser epsilon correction to adjust the degrees of freedom for each test. Post hoc test was made by Bonferroni's multiple comparison test. The threshold for statistical significance was set at $p < 0.05$.

3. Results and discussion

3.1. Formulation and characterization of DA/CSNPs

The ionic gelation technique allowed us to achieve CSNPs by mixing the aqueous CS and TPP solutions (Mao et al., 2010; Trapani et al., 2008, 2010). In preliminary experiments, we attempted to prepare DA/CSNPs by dissolving the neurotransmitter in CS phase but not in the TPP one because DA is sensitive to the strong alkaline conditions of the latter solution. However, according to this approach, negligible DA encapsulation was observed. Therefore, the strategy of the neurotransmitter adsorption onto preformed unloaded CSNPs was selected. In particular, two different concentrations of DA (i.e., 1 and 5 mg/mL) were used to be passively adsorbed onto the surface through the co-incubation of the unloaded carrier for 3 h.

Table 1 displays the physicochemical properties of the different NPs prepared. It is well known that the size of CSNPs depends on the CS and TPP concentrations and the CS/TPP mass ratio (Janes et al., 2001a). However, we observed that DA/CSNPs (1) were quite bigger than the corresponding DA/CSNPs (5) formulations (i.e., 148 (±5) nm average particle size and 110 (±3) nm, respectively (Table 1)). Furthermore, in both cases examined, a broad distribution was noted as proved by the PI values ranging between 0.36 and 0.44. At this stage, the reason behind this decrease in NP size in the presence of 5 mg/mL DA feeding solution is not clear, but our hypothesis is that enhancing the DA amount and consequent adsorption, a conformational reorganization of the polymer occurs leading to NP shrinkage.

In all cases, positive zeta potential values were detected, suggesting that CS chains are mainly located on the surface of the particles. It means that the adhesion and transport properties of the NPs can be facilitated supposing the electrostatic attractions between the positive charged samples and the negatively charged cell membranes. However, it is interesting to note that DA loaded NPs presented lower zeta potential values than CSNPs taken as control (Table 1). This finding may suggest the external localization of DA which should be able to shield the inherent positive charges of CS.

The morphological appearance of the CSNPs was examined by AFM. Fig. 1a and b shows 1 μm × 1 μm topography and phase images, respectively. It is possible to recognize some CSNPs well separated and 20 nm high. Most of these particles seems to be partially aggregated on glass surface probably due to the slow solvent evaporation occurred during the night. On the other hand, the relative phase image seems to be much more clear showing the fine structure of CSNPs. Large area AFM topography image of Fig. 1c highlights the aggregation propensity of CSNPs on glass where very thick nanoparticle islands can be easily found. The size distribution was obtained applying the Watershed algorithm with filter level 1 to a 2.5 μm × 2.5 μm image (Fig. 1d); under this condition CSNPs show 107 nm ± 38 nm of diameter and 10 nm as RMS. Definitely, AFM measurements are in good agreement with PCS data indicating that the CSNPs on glass keep intact their spherical morphology and dimension, even if some aggregates are also noted.

The capacity of DA to be adsorbed on CSNPs was determined by an indirect method removing unbound DA by centrifugation. The determination of the association efficiency of the NPs is based on an indirect way taking into account literature results for other CS-based NPs suggesting that the accuracy of the values determined indirectly is comparable with that based on degradation of the CS with chitosanase (Maestrelli et al., 2006). We observed that by increasing the concentration of DA in the solution incubated, CSNPs association efficiency (AE) also increased [i.e., 32% and 81%, for DA/CSNPs (1) and DA/CSNPs (5), respectively (Table 1)]. The affinity of DA to CS matrix might be related to hydrogen bonding interactions between the $-NH_2$ and –OH groups of CS and the polar groups of DA.

As for the yield values, the most promising formulation for scale up purposes seems to be DA/CSNPs (5) taking into account its yield value greater than that of DA/CSNPs (1) (i.e., 44% and 23%, respectively). It should be noted that Grenha et al. (2005) found yield values around 60% when CS/TPP mass ratio was adjusted to 3.6:1 for NPs based on CS at high molecular weight (i.e., bigger than 100 kDa)

Table 1
Physicochemical properties of unloaded CSNPs and the corresponding DA adsorbing particles. PI: polydispersity index; ζ: zeta potential; EE: association efficiency. Mean ± SD are reported, $n = 6$.

Formulation	Conc. DA (mg/mL)	Size (nm)	PI	ζ (mV)	Association efficiency (%)	Yield (%)
CSNPs	0	98 (±11)	0.36–0.42	+33.9 (±0.4)	0	63 (±12)
DA/CSNPs (1)	1	148 (±5)	0.41–0.44	+23.5 (±0.4)	32 (±7)	23 (±6)
DA/CSNPs (5)	5	110 (±3)	0.38–0.39	+27.0 (±1)	81 (±7)	44 (±12)

(Grenha et al., 2005). The NPs described by the authors were formed after dissolving both the polycation and the polyanion in purified water instead of 0.1% (v/v) of acetic acid employed by us for CS dissolution.

3.2. XPS analysis

XPS has been employed to investigate the surface chemical composition of CSNPs and DA/CSNPs and, in particular, the DA

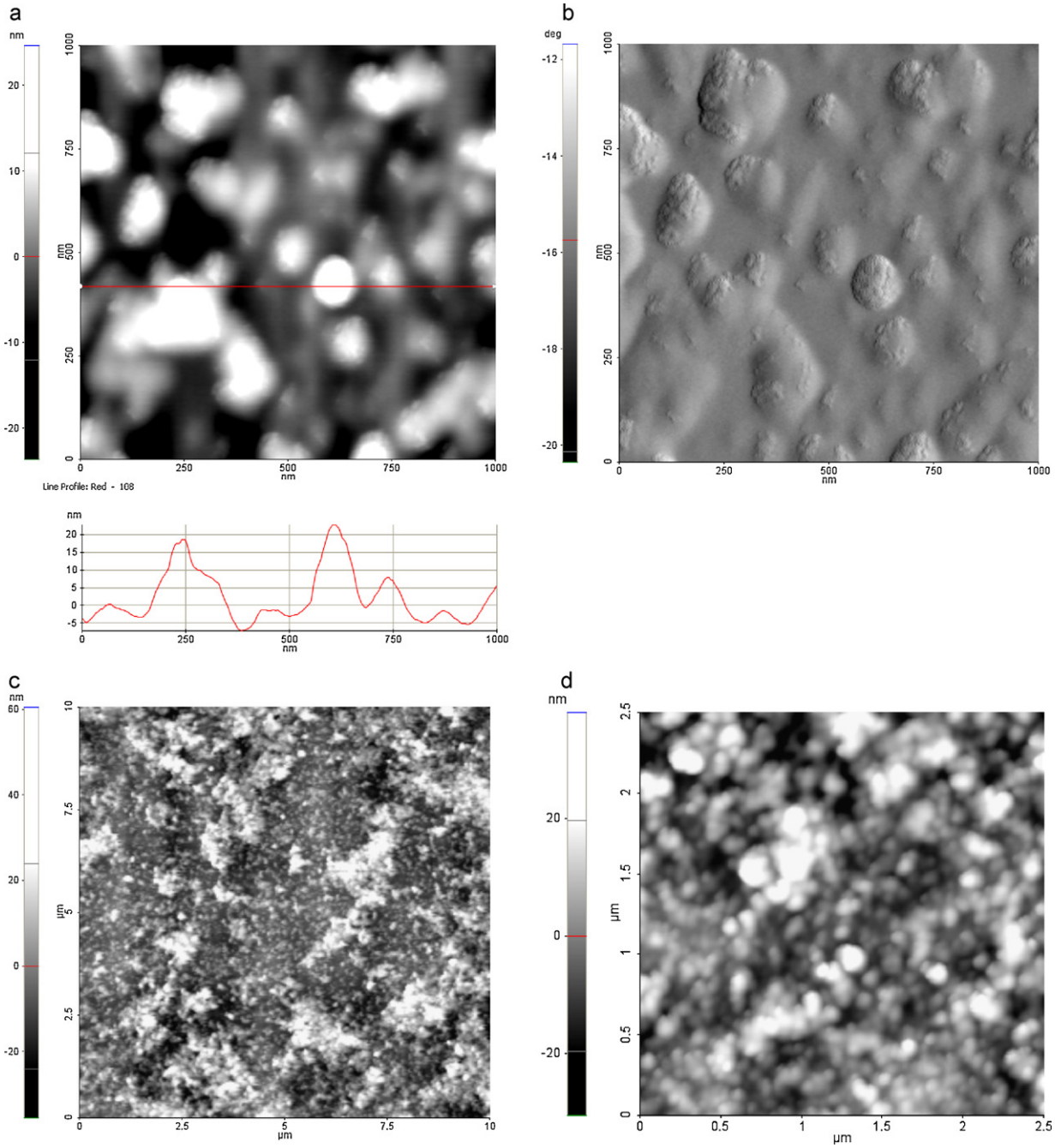

Fig. 1. Atomic force microscopy images of CSNPs [average size by AFM = 107 (±40) nm]. (a) Topography 1 μm × 1 μm and line profile; (b) Phase Image 1 μm × 1 μm of the same region in (a); (c) topography 10 μm × 10 μm; and (d) topography 2.5 μm × 2.5 μm.

Table 2
Peaks position and relative abundance of the C1s peak components relevant to CS, CSNPs, free DA, DA/CSNPs (1) and DA/CSNPs (5). The maximum error on the peak position is ± 0.2 eV.

Attribution	BE (eV)	CS (at.%)	CSNPs (at.%)	DA (at.%)	DA/CSNOS (1) (at.%)	DA/CSNPs (5) (at.%)
A: C–H	285.0	7.5	30.6	62.7	43.0	68.0
B: C–N	285.6	8.0	3.1	–	1.6	–
C: C–O, C–N^+	286.5	64.7	51.2	37.3	43.2	30.7
D: O–C–O	288.0	17.1	13.3	–	10.7	1.3
E: O═C–N	288.9	2.7	1.8	–	1.5	–

localization on the NPs. It should be noted that the adsorption of DA on the CSNPs does not introduce peculiar signals to the XPS spectra but simply adds contributions to carbon, nitrogen and oxygen spectral regions. Therefore, an accurate curve fitting was required in order to check that our preparation procedure of DA/CSNP systems is successful. In Fig. 2, the high-resolution C1s XP spectra of pure CS, CSNPs, free DA, DA/CSNPs (1) and DA/CSNPs (5) were compared. In Table 2, peaks assignments, binding energy (BE) values and relevant atomic percentages were reported. The C1s spectra of CS and CSNPs (Fig. 2a and b) may be split into five peak components associated with the following species: C–H (285.0 eV, ref.), C–N (285.6 eV) C–O and C–N^+ (286.5 eV), O–C–O (288.0 eV) and O═C–N (288.9 eV) of acetyl group. The first peak, attributed to aliphatic carbon, does not belong to CS and expresses contamination of polymer surfaces as a result of adsorbed hydrocarbons monolayers. Two dominant carbon species expected from CS are single-bonded C–O and O–C–O in a ratio 4:1. Indeed, in the C1s spectrum of CS and CSNPs the observed ratio of the components at 286.5 and 288.0 eV is typically 3.8. On the other hand, no XPS literature data are available for free DA. DA C1s spectrum (Fig. 2c) was fitted using two components at 285.0 eV associated to C–H and 286.5 eV associated to C–O and C–N^+ functionalities. The ratio observed between these two peak areas is equal to 1.7 in agreement with the DA stoichiometry. When DA adsorbing CSNPs were examined (Fig. 2a and d), significant differences in C1s spectra can be detected with respect to unloaded CSNPs. As DA concentration grows from 1 to 5 mg/mL, the C1s shape of modified NPs was much more similar to that of the pure neurotransmitter. In particular, the DA adsorption on the CSNPs surfaces leads to an increase of peak at 285.0 eV and a consequent decrease of the other peaks, until CS peaks at 285.6 eV and 288.9 eV disappeared on DA/CSNPs (5). Overall, these findings clearly indicate the DA localization on the CSNPs surface.

The N1s XP spectra of the starting materials, CSNPs and DA/CSNPs were reported in Fig. 3. In Table 3, peaks assignments, BE values and relevant atomic percentages were reported. The N1s regions of CS and CSNPs (Fig. 3a and b) were curve-fitted by three peaks. The lower BE peak (399.6 eV) was attributed to aminic nitrogen, the second one to amide group (401.1 eV) while the higher BE peak was at 402.0 eV and it was due to protonated, quaternary nitrogen. The atomic percentage of the component relevant

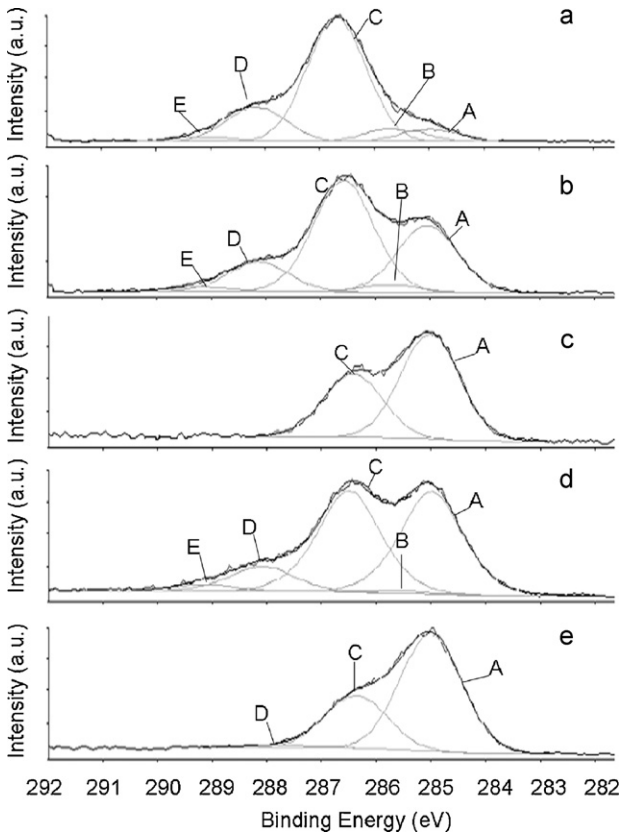

Fig. 2. C1s regions of pure CS (a), CSNPs (b), free DA (c), DA/CSNPs (1) (d) and DA/CSNPs (5) (e). Attribution, binding energies and atomic percentages were reported in Table 3.

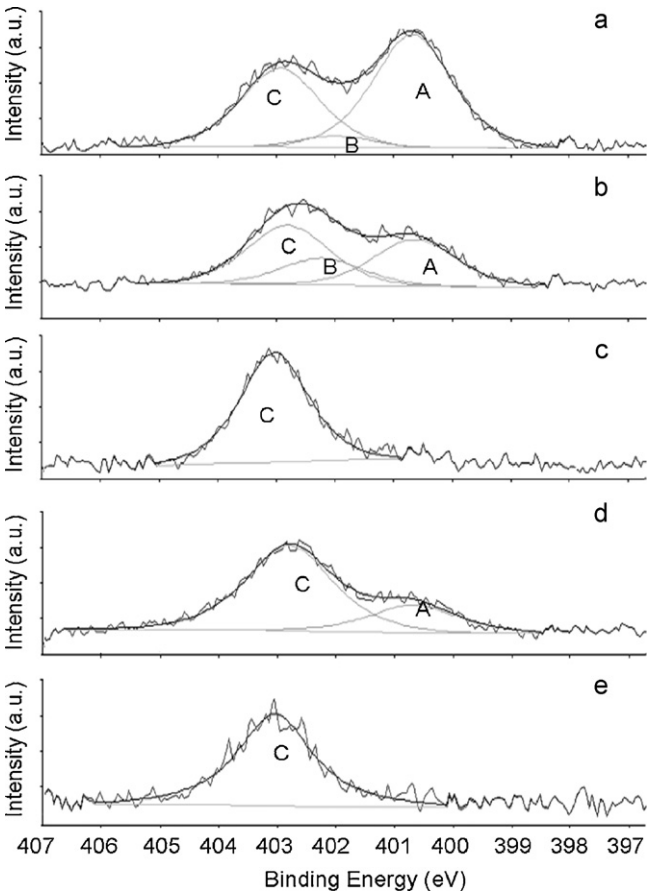

Fig. 3. N1s regions of pure CS (a), CSNPs (b), free DA (c), DA/CSNPs (1) (d) and DA/CSNPs (5) (e). Attributions, binding energies and atomic percentages were reported in Table 4.

Table 3
Peaks position and relative abundance of the N1s peak components relevant to CS, CSNPs, free DA, DA/CSNPs (1) and DA/CSNPs (5). The maximum error on the peak position is ± 0.2 eV.

Attribution	BE (eV)	CS (at.%)	CSNPs (at.%)	DA (at.%)	DA/CSNOS (1) (at.%)	DA/CSNPs (5) (at.%)
A: N–H	399.6	52.4	36.4	–	24.5	–
B: O=C–N	401.1	12.0	13.9	–	–	–
C: N^+–C	402.0	35.6	49.7	100	75.5	100

to amide species can be conveniently used to predict the acetylation degree of CS. Indeed, the obtained percentage was in the range 12–15% of total N1s intensity, in good agreement with the expected deacetylation degree of the CS employed. The different ratios between protonated and aminic nitrogen detected on pure CS and CSNPs can be attributed to the NPs synthesis procedure, leading to protonation of the aminic moieties at low pH conditions. The N1s spectrum of DA (Fig. 3c) showed, as expected, only one component at 402.0 eV attributable to NH_3^+. The N1s signals of DA modified CSNPs (Fig. 3c and d), as in C1s regions, provided a clear evidence of the adsorbing process of DA on the NPs surface. Indeed, increasing DA amount, the percentage of the component at 402.0 eV grows gradually until reaching the 100% on DA/CSNPs (5). It is interesting to note that the absence of an additional peak component at the BE of 398.5 eV attributable to –N= species, in N1s signals of DA modified CSNPs, suggested that DA self-polymerization process did not occur in this case (Liao et al., 2009). The high-resolution O1s spectra of each sample did not add remarkable information to those already obtained from C1s and N1s signals. The O1s regions (data not shown) relevant to all samples, but DA, were curve-fitted by three peaks: the first at 531.5 ± 0.2 eV attributed to inorganic oxides and O=C–N, the second one, at 532.8 ± 0.2 eV, was relative to O–H groups and the third at 533.4 ± 0.2 eV relevant to O–C–O moieties. The latter peak grows in DA modified CSNPs to be predominant in DA/CSNPs (5). On the other hand, DA O1s signal contains, as expected, only one contribute at 533.4 eV. The assignments of the individual spectral components of O1s fit well with those recently published for other CS derivatives (Janciauskaite et al., 2008; Liao et al., 2005). Altogether, XPS analysis suggests that most of DA appears adsorbed on the CSNPs surface rather than dispersed in NPs matrix. Nevertheless, the presence of the neurotransmitter inside the core of NPs cannot be ruled out *a priori*, but the external location of DA could provide a prompt biological availability in the brain. On the other hand, XPS investigation allowed us to point out the marked difference between DA/CSNP (5) and DA/CSNP (1) systems in terms of surface features. Indeed, such a difference cannot be accounted for on the basis of zeta potential values only.

3.3. DA/CSNP (5) formulation stability

A relevant aspect for assessing the performance of nanoparticulate systems *in vivo* is the evaluation of their stability in biological fluids. In particular, it is essential that the NPs maintain their size in physiological medium in view of a possible administration as an injectable formulation. To gain information in this regard, DA/CSNPs (5) were incubated under agitation (100 rpm) in MDCKII-MDR1 cell culture medium as well as in pure water and in microdialysis medium and particle size was monitored by PCS at different incubation times. As shown in Fig. 4, DA/CSNPs (5) suspended in water (used as control) displayed only slight increases in particle size up to 24 h. In contrast, the particles were seen to increase their size (about 550 nm) and polydispersity index (about 0.4–0.5) during 4 h of incubation in the medium used for microdialysis. A similar increase in size was noted when the particles were incubated in MDCKII-MDR1 cell medium for 4 h (data not shown). These particle size increases could result from an aggregation

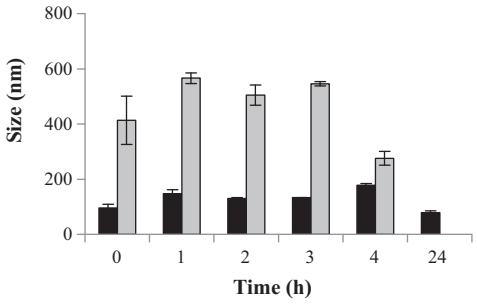

Fig. 4. Size of DA/CSNPs (5) suspended in the medium used for microdialysis studies and incubated at 37 °C. The nanoparticle size was measured at different set time points up to 24 h. Nanoparticle suspension in water at 37 °C was used as control. Data (black bar for suspension in water, grey bar for suspension in the medium used for microdialysis studies) are mean ± SD, $n = 3$.

processes perhaps due to the ionic strength of the medium used as already stated by other authors (Santander-Ortega et al., 2006).

These stability results, although obtained under somewhat stressed conditions (under agitation at 100 rpm), are indicative of a propensity of the nanoparticle suspension to aggregate. Consequently, it can be expected that the formulation will probably release the neurotransmitter *in vivo* with different kinetic than that achieved *in vitro* with a stable nanoparticle suspension.

3.4. In vitro release study

In vitro release tests of NPs were carried out in PBS (pH 7.4) without enzymes and a very different behaviour was observed between DA/CSNPs (1) and DA/CSNPs (5). As shown in Fig. 5, DA/CSNPs (5) exhibited a DA release endowed with an initial burst effect followed by a decreasing release kinetic up to 48 h. On the other hand, DA released from DA/CSNPs (1) was lower and with an almost constant release profile without any burst effect. Maybe it could be due to the fact that, besides the DA in the polymeric matrix, a limited neurotransmitter adsorption on DA/CSNPs (1) occurs, while the DA adsorbed on DA/CSNPs (5) is higher and hence, promptly released. It should be noted that the release profile of DA/CSNPs (5) seems to be suitable for brain DA delivery as its external localization would allow a prompt and pulsate release of DA in the brain. However, a cautionary note should be kept in mind

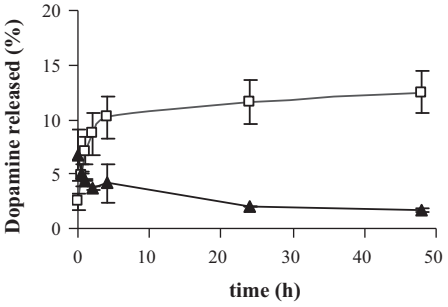

Fig. 5. *In vitro* release profiles of DA/CSNPs in PBS (pH 7.4). Series are DA/CSNPs (1) (▲) and DA/CSNPs (5) (□).

Table 4
IC_{50} free DA-, unloaded CS NPs- and DA adsorbing NPs-induced cytotoxicity in MDCKII-MDR1 cells. The cells were treated with free DA, CSNPs and DA/CSNPs for 3 h and 24 h. The cell viability was measured via the MTT assay and compared to a control (i.e., free DA at 3 h and free DA at 24 h). Values represent mean ± SEM ($n = 6$).

Formulation	Time of exposure (h)	IC_{50} (μg/mL) in MDCKII-MDR1 cell line
DA/CSNPs (1)	24	42 (±4)[a]
DA/CSNPs (5)	24	5×10^{-2} (±0.04)
CSNPs	24	3×10^{-2} (±0.01)
Free DA	24	4×10^{-2} (±0.01)
DA/CSNPs (1)	3	6×10^{-3} (±0.004)
DA/CSNPs (5)	3	1.5×10^{-3} (±0.0009)
CSNPs	3	0.10 (±0.03)[a]
Free DA	3	3×10^{-4} (±0.0002)

[a] Significantly different from the control ($p < 0.001$).

in view of *in vivo* experiments. In fact, starting from 6 h of exposure, grey samples evolving to black ones later on were observed throughout the study leading us to full stop the *in vitro* release studies after 48 h. Likely, it is related to the oxidation of the neurotransmitter with the formation of quinone intermediates. On the other hand, it is also true that release conditions are expected to change dramatically *in vivo* and DA release process could be triggered in a quicker way than predicted from *in vitro* release tests.

3.5. Cell viability studies

MDCKII-MDR1 are cells originating from dog renal distal tubular epithelium transfected with the human MDR1 gene encoding for P-gp and they are recommended as a model of *in vitro* human BBB (Puttonen et al., 2006; Mensch et al., 2009). In fact, on the apical membranes of MDCKII-MDR1 cells not only the efflux pump P-gp is overexpressed but also a quite high transepithelial electric resistance makes them a potentially attractive model for *in vitro* screening BBB permeability of drugs.

Firstly, the evaluation of the cytotoxic effect of the CSNPs and DA/CSNPs was performed according to the MTT test, by incubating the samples for 3 h (the reasonable frame time for *in vitro* transport studies aiming at simulate the overcoming of the BBB) and 24 h, according to the well-known protocols of MTT test (Hansen et al., 1989).

It was found that, except for unloaded CSNPs, the IC_{50} values of free DA and DA/CSNPs increased in a time dependent manner, as shown in Table 4. To account for this finding, we suppose that for free DA and DA/CSNPs cell proliferation occurring in the long range of 24 h might be able to compensate the cell death due to the intrinsic toxicity of the neurotransmitter (Hanrott et al., 2006), so making the same particles safer when incubated for 24 h rather than for 3 h. Conversely, the toxicity of CSNPs results in good agreement with Diebold et al. findings (2007) for CS based NPs who suggested that the cells are more viable after 3 h rather than 24 h because they need a certain amount of time to perform metabolic processes necessary to adapt the contact with exogenous materials like CSNPs.

From the evaluation of the intrinsic cytotoxic effects of DA/CSNPs and free DA, it was evident that the nanovectors are less cytotoxic [i.e., IC_{50} values of 42 and 5×10^{-2} vs. 4×10^{-2}, for DA/CSNPs (1), DA/CSNPs (5) and free DA, respectively]. Furthermore, the higher cytotoxicity displayed by DA/CSNPs (5) rather than DA/CSNPs (1) seems most likely due to their higher positive zeta potential and hence more intense cell interactions.

3.6. Transport of CSNPs across MDCKII-MDR1 monolayer

The assessment of cytotoxicity by MTT test was a preliminary test to transport studies of NPs across MDCKII-MDR1 cell monolayer, taken as an *in vitro* model of BBB. We aimed to predict the supply of the neurotransmitter adsorbed onto the particles to the brain compartment within an average time of 3 h which appeared a suitable frame time according to *in vitro* release assay. Firstly, the interaction of FITC-DA/CSNPs (5) and MDCKII-MDR1 cells was evaluated by flow cytometry and a significant and gradual fluorescence intensity increase within 180 min was detected (Fig. 6a). In fact, the mean cellular fluorescence intensity of FITC-DA/CSNPs (5) treated cells increased 2.4-fold after 15 min, 6.2-fold after 60 min and 12-fold after 180 min compared to untreated cells which did not exhibit significant background fluorescence. This result cannot be interpreted as an unambiguous evidence that the particles are taken-up from the cells. In order to prove the delivery of CSNPs into MDCKII-MDR1 cells, unloaded FITC-CSNPs were prepared and incubated with that cells up to 4 h and then observed by fluorescence microscopy. As shown in Fig. 6b, when MDCKII-MDR 1 cells were individually treated with 8 μM of NPs (the concentration is referred to FITC) after 4 h a clear punctuate green fluorescence appeared localized in the cytosol but none in the nucleus of the cells. It clearly proved that the internalized fluorescence of the cells was due to the cellular uptake of the particles. If NPs fluorescence is compartmentalized into specific subcellular organelles deserves further investigations. To further support the internalization of CSNPs, the transport across MDCKII-MDR1 cell line monolayer of FITC labelled unloaded CSNPs was investigated. It was found an ever increasing fluorescence intensity in basolateral chamber during the period of the experiment. It can be referred to FITC-CSNPs (assuming that no hydrolysis occurred at level of the dye moiety and CSNPs) and/or to free FITC permeated. Altogether, these results may suggest that the interaction, electrostatic in nature, between polycationic CS and negative charges on the cell monolayer

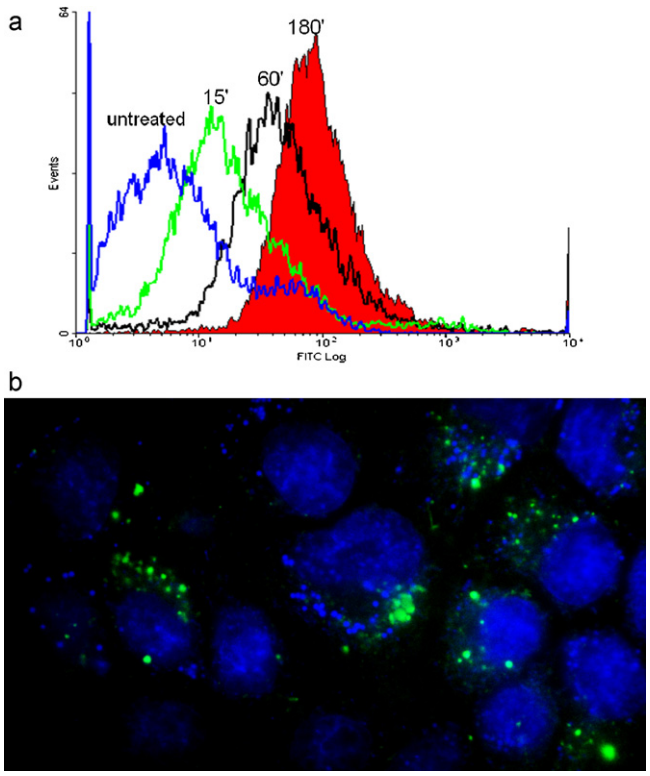

Fig. 6. (a) Flow cytometry of the cell entry dynamics of FITC-DA/CSNPs (5) in MDCKII-MDR1 cells. The log of FITC absorption intensity (on *x*-axis) is plotted against the number of cells (counts of *y*-axis). The increase in the interaction between FITC-DA/CSNPs (5) and MDCKII-MDR1 cells within 15 min compared to untreated cells is evident. (b) Fluorescence microscopy image showing the deliver of unloaded FITC-CSNPs into MDCKII-MDR1 cells.

Table 5
Apparent permeability coefficient (P_{app}) of DA (A) and FD4 (4000 M_w) (B) determined in MDCKII-MDR1 monolayers exposed to free DA, DA/CSNPs (1) and DA/CSNPs (5). Data are mean ± SD, $n = 5$.

Treatment	P_{app} DA ($\times 10^{-7}$ cm/s)	Relative P_{app} (carrier/control)
(A)		
Free DA	1.31 ± 0.16	–
DA/CSNPs (1)	1.22 ± 0.57	–
DA/CSNPs (5)	3.27 ± 0.81[a]	2.5
Treatment	P_{app} FD4 ($\times 10^{-7}$ cm/s)	Relative P_{app} (carrier/control)
(B)		
Free DA	0.25 ± 0.11[b]	–
DA/CSNPs (1)	0.88 ± 0.78	–
DA/CSNPs (5)	1.70 ± 0.13	1.3
FD4	1.35 ± 0.48	–

[a] $p < 0.001$ compared to free DA.
[b] $p < 0.05$ compared to FD4.

surface influences the transport supporting so the hypothesized AMT mechanism.

As a following step, the quantitative evaluation of the transport of DA across MDCKII-MDR1 cells was performed prior to *in vivo* particles administration to the rats. Generally, it is well known that CS is capable of opening the tight junctions of epithelial cells (Janes et al., 2001b). In several works, indeed, CS has been shown to improve the intestinal epithelium penetration. However, whether or not particles prepared from CS maintain their intrinsic capacity to modify the permeability of cell monolayers still remains unknown. Thus, in the present work, we found it important to determine if the association of CSNPs and DA has a consequence in terms of MDCKII-MDR1 cell monolayer permeability. Importantly, DA/CSNPs (5) were seen to increase DA permeability of 2.5-fold than free DA as reported in Table 5A. The apparent permeability coefficient value (P_{app}) of DA found in this work was not statistically different from that already observed (Denora et al., 2007). Moreover, the enhanced permeability effect observed for DA/CSNPs (5) greater than the corresponding DA/CSNPs (1) may be ascribed to the smaller size of the former. The measurement of the transepithelial electric resistance (TEER) is a common way to determine the paracellular permeability to ions and their changes upon exposure to a permeation enhancer (Bonferoni et al., 2008). This information is relevant as reductions in the TEER can be correlated with partial disruption of the tight junction complex that restricts the paracellular route for hydrophilic compounds. In the present study, no significant changes were appreciated in TEER values of the monolayers exposed to free DA in the control wells (Fig. 7a). On the other hand, DA/CSNPs DA (1) and DA/CSNPs (5) presented a different behaviour compared to that of control wells. More specifically, the TEER values of the monolayers exposed to DA/CSNPs decreased continuously during the experiment (3 h). Then, after removal of the nanoparticle formulations from the apical side, the monolayers were washed and incubated with DMEM and further incubated for the next 24 h. During this period, a slow recuperation of the TEER values was observed, reaching about the 80% of recuperation. The P_{app} value of the fluorescent marker FD4 (4000 M_w) was in good agreement with the TEER data (Table 5B). The results showed that neither free DA nor DA/CSNPs (1) have a permeability enhancing effect toward FD4. In contrast, DA/CSNPs (5) elicited a slight transport enhancing effect compared with the control. Indeed, the permeability values were almost 1.3-fold greater than those of the control (FD4) and it means an about 30% increase in permeability. Overall, this permeability enhancing effect seems to be modest and therefore it cannot support the hypothesis of a paracellular transport mechanism for DA/CSNPs (5).

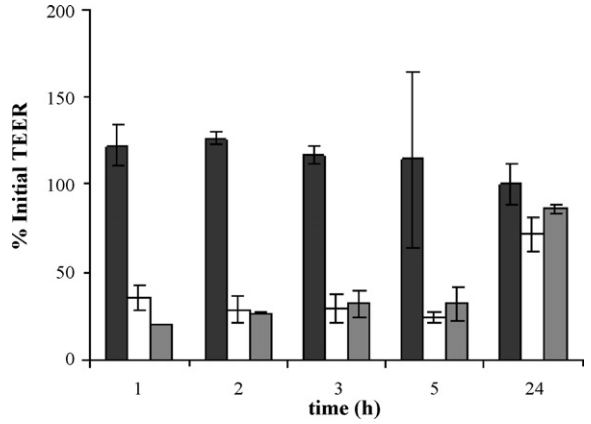

Fig. 7. Transepithelial electric resistance (TEER) of MDCKII-MDR1 monolayers exposed to samples. Black, white and grey bars refer to free DA, DA/CSNPs (1) and DA/CSNPs (5), respectively. Data are mean ± SD, $n = 5$.

3.7. ROS production in MDCKII-MDR1 monolayer

To evaluate the potential neurotoxic effect of the carriers (i.e., CSNPs) and drug loaded particles (i.e., DA/CSNPs), the analysis of intracellular ROS production was carried out. As shown in Fig. 8, the intracellular ROS production induced by 100 μM of 6-OHDA was dependent on the incubation time between MDCKII-MDR1 cells/samples. When the exposure cells-DA/CSNPs was performed for 3 h, in contrast to that observed for CSNPs, some effect to prevent the ROS elevation was measured for drug loaded particles ($p < 0.001$ and $p < 0.01$ for DA/CSNPs (1) and DA/CSNPs (5), respectively). On the other hand, ROS production increased in comparison to 6-OHDA-treated cells only when the cells were preincubated with DA/CSNPs (5) for 24 h ($p < 0.001$). These findings may be related to the oxidation of the neurotransmitter occurring after prolonged incubation times. As for the neurotoxic effect of the unloaded carriers, no statistical significant difference in terms of ROS production

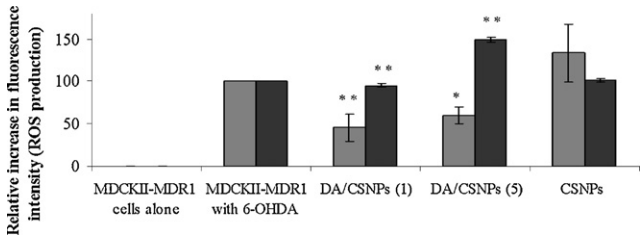

Fig. 8. Intracellular ROS formation in the presence of different CSNPs. Grey and black bars refer to 3 h and 24 h of contact cells/samples, respectively. Data are mean ± SEM, $n = 6$. $^{*}p < 0.01$ and $^{**}p < 0.001$ compared to 6-OHDA-treated cells using one-way ANOVA with Bonferroni's post hoc test.

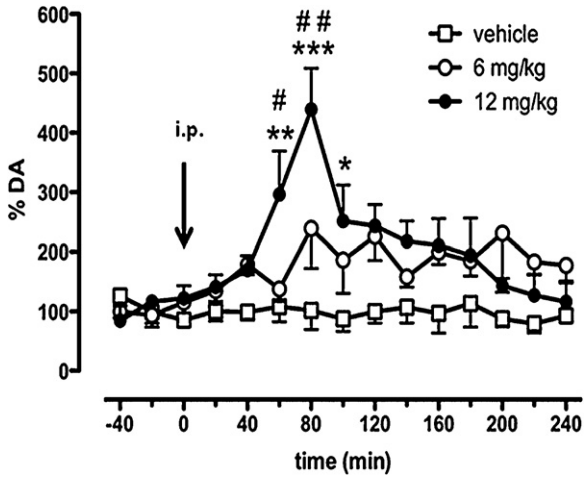

Fig. 9. Effect of single (6–12 mg/kg, i.p.) DA/CSNPs (5) injections on DA outflow over 4 h in striatum of awake rats. Data are expressed as percentages of baseline (±SEM) of $n = 4$ animals per group. Two-way ANOVA followed by Bonferroni's multiple comparison test. $^{*}p < 0.05$, $^{**}p < 0.01$, $^{***}p < 0.001$ vs. respective vehicle; $^{\#}p < 0.05$, $^{\#\#}p < 0.01$ vs. respective DA/CSNPs (5) (6 mg/kg). Arrow indicates the time of DA/CSNPs (5) or vehicle (CSNPs) administration.

was detected between CSNPs and 6-OHDA-treated cells at both 3 and 24 h. From these results it may be concluded that DA/CSNPs seem promising DA carriers because in the frame time of 3 h they reduce ROS production.

3.8. Effects of DA/CSNPs (5) administration on striatal DA output

To assess whether the administration of DA/CSNPs (5) influences brain dopaminergic transmission, we measured the extracellular output of DA in the striatum of freely moving rats by microdialysis. The effects of a single injection (6–12 mg/kg, i.p.) of DA/CSNPs (5) on the basal extracellular concentrations of DA (440 ± 62 pg/mL) were determined for 4 h after administration of the drug (Fig. 9). Two-way ANOVA revealed a significant main effect of treatment [$F_{2,9} = 10.610$, $p < 0.01$]; a significant main effect of repeated measures: [$F_{14,126} = 4.336$, $p < 0.01$] and a significant interaction between factors [$F_{28,126} = 2.413$, $p < 0.05$]. The post hoc test showed that DA/CSNPs (5), administered i.p. at the dose of 12 mg/kg, induced a significant increase in extracellular DA concentrations that peaked (439% increase above the baseline) 80 min after treatment and disappeared within 120 min. Following the administration of the lowest dose of DA/CSNPs (5) (6 mg/kg), we observed a trend toward an increase of striatal DA level, which was maximal (+239% above the baseline) at 80 min after administration, although it did not reach the statistical significance. No effect was observed after vehicle (CSNPs, i.p.) administration. These *in vivo* results are consistent with the *in vitro* drug release studies suggesting a prompt and pulsate release of DA from DA/CSNPs (5).

4. Conclusions

In this study, NPs consisting of CS have been prepared and characterized *in vitro* as potential formulations for brain DA delivery. The neurotransmitter has been externally adsorbed and, when DA feeding solution was set at 5 mg/mL, DA/CSNPs (5) were obtained with satisfactory association efficiency value (i.e., 81%, greater than the one previously reported (Pillay et al., 2009)). XPS analysis helped us to fully understand the external organization of this nanocarrier system. Labelled unloaded CSNPs were seen by fluorescence microscopy experiments to be taken up by MDCKII-MDR1 cells. It was also found that using DA/CSNPs (5) an improvement of DA transport across the cells and reduction of ROS production after 3 h occur. Microdialysis studies showed that the DA/CSNPs (5) induce a dose- and time-dependent increase of DA levels in the rat striatum. Thus, these NPs seem useful for DA delivery to the brain because they could transport the neurotransmitter across BBB. As for the transport mechanism of CSNPs across the BBB, no definitive conclusions can be drawn but, at this stage, our hypothesis that AMT may be involved cannot be ruled out. Indeed, among the mechanisms involved in the internalization of nanodevices including carrier-mediated transport (CMT), RMT and AMT (Paolino et al., 2011) only this last pathway seems to be plausible. It follows from the consideration that neither carriers nor specific binding sites for the polycationic CS are known. An experimental evidence that supports the AMT mechanism is constituted from the observed uptake into and transport study across the MDCKII-MDR1 cells of labelled unloaded CSNPs. Of course, the effect of additional factors including the polymer molecular weight and the cationic charge density should be considered in order to substantiate further the AMT process.

Comparing the *in vivo* drug release from the DA/CSNPs (5) with that from DA-loaded cellulose acetate phthalate NPs (Pillay et al., 2009), it results that DA-loaded cellulose acetate phthalate implants produces a peak after 3 days and thereafter provides a sustained DA release for 30 days. However, such release profile may cause greater neurotoxicity than that brought about from a pulsate drug release system such as DA/CSNPs (5). Thus, DA/CSNPs (5) constitute interesting carrier systems with desirable features for DA brain delivery, taking also into account that they are administered by a less invasive route than the intratecal implant already proposed (Pillay et al., 2009) and, hence, may be useful for the PD treatment.

Acknowledgements

This project was financed by Università degli Studi di Bari (Progetti d'Ateneo to E. De Giglio and G. Trapani) and MIUR (Ministero dell'Istruzione, dell'Università e della Ricerca) to G. Trapani. We thank Dr. Stefania Cometa for helpful discussion and Dr. Massimo Lasorsa for his valuable help with fluorescence microscopy studies. The authors gratefully thank Dr. Giuliano Iacobellis for the AFM characterization. The AFM instrument has been acquired within the framework of Regional Laboratory for Novel-nano and biotechnologies of water filtration (WAFITECH) financially supported by Regione Puglia (Italy).

References

Bonferoni, M.C., Sandri, G., Rossi, S., Ferrari, F., Gibin, S., Caramella, C., 2008. Chitosan citrate as multifunctional polymer for vaginal delivery Evaluation of penetration enhancement and peptidase inhibition properties. Eur. J. Pharm. Sci. 33, 166–176.

Cassano, T., Gaetani, S., Morgese, M.G., Macheda, T., Laconca, L., Dipasquale, P., Taltavull, J., Shippenberg, T.S., Cuomo, V., Gobbi, G., 2009. Monoaminergic changes in locus coeruleus and dorsal raphe nucleus following noradrenaline depletion. Neurochem. Res. 34, 1417–1426.

Cho, K., Wang, X., Nie, S., Chen, Z., Shin, D.M., 2008. Therapeutic nanoparticles for drug delivery in cancer. Clin. Cancer Res. 14, 1310–1316.

Csaba, N., Garcia-Fuentes, M., Alonso, M.J., 2006. The performance of nanocarriers for transmucosal drug delivery. Expert Opin. Drug Del. 3, 463–478.

Denora, N., Laquintana, V., Lopedota, A., Serra, M., Dazzi, L., Biggio, G., Pal, D., Mitra, A.K., Latrofa, A., Trapani, G., Liso, G., 2007. Novel L-Dopa and dopamine prodrugs containing a 2-phenylimidazopyridine moiety. Pharm. Res. 24, 1309–1324.

Demirel, M., Yazan, M., Muller, R.H., Kilic, F., Bozan, B., 2001. Formulation and in vitro–in vivo evaluation of piribedil solid lipid micro and nanoparticles. J. Microencapsul. 18, 359–371.

Diebold, Y., Jarrin, M., Saez, V., Carvalho, E.L.S., Orea, M., Calonge, M., Seijo, B., Alonso, M.J., 2007. Ocular drug delivery by liposome–chitosan nanoparticle complexes (LCS-NPs). Biomaterials 28, 1553–1564.

Du, Y., Ding, Y., Sun, M., Zhang, L., Jiang, X., Yang, C., 2007. Hollow chitosan/poly(acrylic acid) nanospheres as drug carriers. Biomacromolecules 8, 1069–1076.

Enoch, W.S., Sarna, T., Zecca, L., Riley, P.A., Swartz, H.M., 1994. The roles of neuromelanin, binding of metal ions, and the oxidative cytotoxicity in the pathogenesis of Parkinson's disease: a hypothesis. J. Neural Transm. 7, 83–100.

Gaillard, P.J., de Boer, A.G., 2000. Relationship between permeability status of the blood–brain barrier and in vitro permeability coefficient of a drug. Eur. J. Pharm. Sci. 12, 95–102.

Grenha, A., Seijo, B., Remunan-Lopez, C., 2005. Microencapsulated chitosan nanoparticles for lung protein delivery. Eur. J. Pharm. Sci. 25, 427–437.

Hanrott, K., Gudmunsen, L., O'Neill, M.J., Wonnacott, S., 2006. 6-Hydroxydopamine-induced apoptosis is mediated via extracellular auto-oxidation and caspase 3-dependent activation of protein kinase Cdelta. J. Biol. Chem. 281, 5373–5382.

Hansen, M., Nielsen, S., Berg, K., 1989. Re-examination and further development of a precise and rapid dye method for measuring cell growth/cell kill. Immunol. Methods 119, 203–210.

Hervé, F., Ghinea, N., Scherrmann, J.M., 2008. CNS delivery via adsorptive transcytosis. AAPS J. 10, 455–472.

Janciauskaite, U., Rakutyte, V., Miskinis, J., Makuska, R., 2008. Synthesis and properties of chitosan-N-dextran graft copolymers. React. Funct. Polym. 68, 787–796.

Janes, K.A., Calvo, P., Alonso, M.J., 2001a. Polysaccharide colloidal nanoparticles as delivery systems for macromolecules. Adv. Drug Del. Rev. 47, 83–97.

Janes, K.A., Fresneau, M.P., Marazuela, A., Fabra, A., Alonso, M.J., 2001b. Chitosan nanoparticles as delivery systems for doxorubicin. J. Control. Release 73, 255–267.

Jellinger, K., Linert, L., Kienzl, E., Herlinger, E., Youdin, M.B., 1995. Chemical evidence for 6-hydroxydopamine to be a endogenous toxic factor in the pathogenesis of Parkinson's disease. J. Neural Transm. 46, S293–S310.

Ieva, E., Trapani, A., Cioffi, N., Ditaranto, N., Monopoli, A., Sabbatini, L., 2009. Analytical characterization of chitosan nanoparticles for peptide drug delivery applications. Anal. Bioanal. Chem. 393, 207–215.

Liao, Y., Cao, B., Wang, W.C., Zhang, L.Q., Wu, D.Z., Jin, R.G., 2009. A facile method for preparing highly conductive and reflective surface-silvered polyimide films. Appl. Surf. Sci. 255, 8207–8212.

Liao, J.D., Lin, S.P., Wu, Y.T., 2005. Dual properties of the deacetylated sites in chitosan for molecular immobilization and biofunctional effects. Biomacromolecules 6, 392–399.

Lopedota, A., Trapani, A., Cutrignelli, A., Chiarantini, L., Pantucci, E., Curci, R., Manuali, E., Trapani, G., 2009. The use of Eudragit RS 100/cyclodextrin nanoparticles for the transmucosal administration of glutathione. Eur. J. Pharm. Biopharm. 72, 509–520.

Maestrelli, F., Garcia-Fuentes, M., Mura, P., Alonso, M.J., 2006. A new drug nanocarrier consisting of chitosan and hydroxypropylcyclodextrin. Eur. J. Pharm. Biopharm. 63, 79–86.

Mao, S., Sun, W., Kissel, T., 2010. Chitosan-based formulations for delivery of si-RNA and DNA systems for protein therapeutics and antigens. Adv. Drug Del. Rev. 62, 12–27.

Mensch, J., Oyarzabal, J., Mackie, C., Augustijns, P., 2009. In vivo, in vitro and in silico methods for small molecule transfer across BBB. J. Pharm. Sci. 98, 4429–4468.

Pahwa, R., Koller, W.C., 1998. Advances in the treatment of Parkinson disease. Drugs Today 34, 95–105.

Paolino, D., Cosco, D., Molinaro, R., Celia, C., Fresta, M., 2011. Supramolecular devices to improve the treatment of brain diseases. Drug Discov. Today 16, 311–324.

Park, J., Han, T.H., Lee, K.Y., Han, S.S., Hwang, J.J., Moon, D.H., Kim, S.Y., Cho, Y.W., 2006. N-acetyl histidine-conjugated glycol chitosan self assembled nanoparticles for intracytoplasmic delivery of drugs: endocytosis, exocytosis and drug release. J. Control. Release 115, 37–45.

Paxinos, G., Watson, C.R.R., 1998. The Rat Brain in Stereotaxic Coordinates. Elsevier Academic Press, New York.

Pillay, S., Pillay, V., Choonara, Y.E., Naidoo, D., Khan, R.A., du Toit, L.C., Ndesendo, V.M.K., Modi, G., Danckwerts, M.P., Iyuke, S.E., 2009. Design, biometric simulation and optimization of a nano-enabled scaffold device for enhanced delivery of dopamine to the brain. Int. J. Pharm. 382, 277–299.

Pinnen, F., Cacciatore, I., Cornacchia, C., Sozio, P., Iannitelli, A., Costa, M., Pecci, L., Nasuti, C., Cantalamessa, F., Di Stefano, A., 2007. Synthesis and study of L-Dopa-glutathione codrugs as new anti-Parkinson agents with free radical scavenging properties. J. Med. Chem. 50, 2506–2515.

Puttonen, K.A., Lehtonen, S., Raasmaja, A., Mannisto, P.T., 2006. A prolyl oligopeptidase inhibitor Z-Pro-Prolinal, inhibits glyceraldehyde-3 phosphate dehydrogenase translocation and production of reactive oxygen species in CV1-P cells exposed to 6-hydroxydopamine. Toxicol. In Vitro 20, 1446–1454.

Santander-Ortega, M.J., Jodar-Reyes, A.B., Csaba, N., Bastos-Gonzalez, D., Ortega-Vinuesa, J.L., 2006. Colloidal stability of Pluronic F68-coated PLGA nanoparticles: a variety of stabilisation mechanisms. J. Colloid Interface Sci. 302, 522–529.

Sheetal, S., Babbar, A.K., Sharma, R.K., Tanima, B., Amarnath, M., 2005. Pharmacoscintigraphic evaluation of polysorbate80-coated chitosan nanoparticles for brain targeting. Am. J. Drug Del. 3, 205–212.

Trapani, A., Garcia-Fuentes, M., Alonso, M.J., 2008. Novel drug nanocarriers combining hydrophilic cyclodextrins and chitosan. Nanotechnology 19, 185101/1–185101/10.

Trapani, A., Lopedota, A., Franco, M., Cioffi, N., Ieva, E., Garcia-Fuentes, M., Alonso, M.J., 2010. A comparative study of chitosan and chitosan/cyclodextrin nanoparticles as potential carriers for oral delivery of small peptides. Eur. J. Pharm. Biopharm. 75, 26–32.